HHS Public Access

Author manuscript

Immunity. Author manuscript; available in PMC 2016 March 17.

Published in final edited form as:

Immunity. 2015 March 17; 42(3): 524–537. doi:10.1016/j.immuni.2015.02.009.

CXCR3 Chemokine Receptor Enables Local CD8+ T Cell Migration for the Destruction of Virus-Infected Cells

Heather D. Hickman[1,*], **Glennys V. Reynoso**[1], **Barbara F. Ngudiankama**[1], **Stephanie S. Cush**[1], **James Gibbs**[1], **Jack R. Bennink**[1], and **Jonathan W. Yewdell**[1]

[1]Cell Biology and Viral Immunology Sections, Laboratory of Viral Diseases, National Institutes of Allergy and Infectious Diseases, National Institutes of Health, Bethesda, MD 20892.

SUMMARY

CD8$^+$ T cells play a critical role limiting peripheral virus replication, yet how they locate virus-infected cells within tissues is unknown. Here, we have examined the environmental signals that CD8$^+$ T cells use to localize and eliminate virus-infected skin cells. Epicutaneous vaccinia virus (VV) infection, mimicking human smallpox vaccination, greatly increased expression of the CXCR3 chemokine receptor ligands CXCL9 and -10 in VV-infected skin. Despite normal T cell numbers in the skin, *Cxcr3*$^{-/-}$ mice exhibited dramatically impaired CD8$^+$ T cell-dependent virus clearance. Intravital microscopy revealed that *Cxcr3*$^{-/-}$ T cells were markedly deficient in locating, engaging, and killing virus-infected cells. Further, transfer of wild-type CD8$^+$ T cells restored viral clearance in *Cxcr3*$^{-/-}$animals. These findings demonstrate a function for CXCR3 in enhancing the ability of tissue-localized CD8$^+$ T cells to locate virus-infected cells and thereby exert anti-viral effector functions.

INTRODUCTION

Viral infections of vertebrates typically begin in mucosal surfaces or the skin, where virions can be introduced by insect bites or directly into cuts or abrasions. Locally released virions often infect adjacent cells but can potentially spread distally via the blood or lymphatics. Viral proteins are delivered to draining lymph nodes (DLNs) as free virions, sub-virion forms, or by antigen presenting cells (APCs) that are either infected with the virus or are cross-presenting viral proteins that they have acquired from other cells. Within DLNs, naïve CD8$^+$ T cells survey infected or cross-presenting APCs. Cognate T cells become activated, proliferate, and traffic to peripheral infected tissues to resolve virus infection through a variety of effector mechanisms, including lysing infected cells and releasing antiviral cytokines (Gordon et al., 2011; Liu et al., 2010; Mota et al., 2011).

*Correspondence to: Heather D. Hickman, hhickman@mail.nih.gov, 301-496-2468.

Recent intravital multiphoton microscopy (MPM) studies into the *in vivo* function of effector $CD8^+$ T cells have focused on priming in the DLNs, providing great insight into the events leading to naïve T cell activation (for reviews see (Henrickson and von Andrian, 2007; Hickman et al., 2011a; Mueller and Hickman, 2010)). Less is known about how $CD8^+$ T cells exert their anti-viral functions during active primary infections in the tissue. Using a vaccinia virus (VV) mouse ear infection model, we defined a central role for $CD8^+$ T cells in clearing mobile virus-infected inflammatory monocytes (Hickman et al., 2013). Though adept at eliminating this subset of infected cells, $CD8^+$ T cells only reluctantly entered compact foci of VV-infected keratinocytes. Thus, highly selective interactions coordinate viral clearance in the tissue.

It is currently unclear how antiviral effector $CD8^+$ T cells locate and further select particular infected cells within a complex tissue environ, however chemokines often shape cellular movement through a number of mechanisms. Ligation of soluble chemokine to the cognate receptor leads to integrin activation essential for the stable adhesion required for transmigration through inflamed vessels (the role of integrins in interstitial migration is more varied) (Friedl and Weigelin, 2008; Lammermann et al., 2008; Overstreet et al., 2013). Diffusible chemokine gradients induce cellular chemotaxis *in vitro*, while *in vivo* chemokines may also be bound to extracellular matrix components (ECM) and displayed on cell surfaces, thereby promoting cell-cell interactions (Hsieh et al., 2006; Proudfoot et al., 2003; Rot, 1993). Chemokine deficiencies lead to enhanced susceptibility to many viral infections in both mice and humans, indicating an important role for chemokine-guided migration in the mitigation of virus-induced pathology (Lim and Murphy, 2011). Though chemokines clearly aid in the entry of immune effectors into infected tissue, their role after cellular entry in shaping migration patterns *in situ* has not been established during viral infection.

Here, we examined the role of chemokines during cytotoxic T lymphocyte (CTL) “hunting” of virus-infected cells. Since viruses can cleverly manipulate gene expression in infected cells, it is possible that they control chemokine secretion to prevent detection, enhancing replication and ultimately, host transmission. We imaged T cell location, movement and function in VV-infected skin, defining a novel role for CXCR3 ligands in $CD8^+$ T cell recognition and killing of virus-infected cells.

RESULTS

Activated T Cells Contact Peripheral Virus-Infected Cells Lacking Cognate Antigen

We previously reported that after epicutaneous (ec.) recombinant (TK^-) vaccinia virus (VV) inoculation, most infected cells in the skin are either $LY6C^+$ inflammatory monocytes or keratinocytes (Hickman et al., 2013). Activated antigen (Ag)-specific $CD8^+$ T cells migrate into the tissue and principally focus on killing infected monocytes rather than keratinocytes (Hickman et al., 2013). To better understand how $CD8^+$ T cells locate virus-infected cells, we first examined the contribution of cognate antigen to T cell behavior in VV-infected skin.

Twelve hours (hr.) after adoptively transferring 2.5×10^5 dsRed OT-I T cell-receptor transgenic $CD8^+$ T cells (red, specific for K^b-SIINFEKL) into albino C57BL/6 mice, we

inoculated mice epicutaneously (ec.) in one ear with VV-NP-S-eGFP (which expresses SIINFEKL fused to a nuclear-targeted fluorescent protein (Hickman et al., 2011b; Hickman et al., 2008)); and in the other ear with VV-NP-eGFP (same construct lacking SIINFEKL) (**Figure 1A**). Initially, we enumerated OT-I $CD8^+$ T cells in ears and draining lymph nodes (LNs) at days 1 through 8 post-infection (p.i.) which spanned the infectious process from the first few infected cells to complete resolution in most cases (Hickman et al., 2013) (**Figure 1B**). OT-I $CD8^+$ T cells increased greatly (from ~150 to 600,000) in the LN draining the VV-NP-S-eGFP infected ear, with less OT-I cells recovered from the non-cognate antigen (VV-NP-eGFP) LN at each time point. Despite the SIINFEKL-dependent disparity in T cell numbers in LNs, cognate antigen had little effect on OT-I T cell numbers in the ear (**Figure 1B, right panel**). Importantly, OT-I T cells were not recruited to uninfected ears (**Figure S1**). Thus, VV-induced skin inflammation *per se* is sufficient to recruit activated T cells in the absence of cognate Ag.

How does cognate antigen affect OT-I $CD8^+$ T cell entry to virus-inflamed skin? MPM imaging ears 5-7 p.i. revealed that antigen is was not required for OT-I cells to locate and surround keratinocytic foci of virus replication (**Figure 1C**) or infected inflammatory monocytes (**Figure 1D).** Cognate antigen was clearly required, however, for T cells to stably interact with infected monocytes: in the absence of SIINFEKL, OT-I cells quickly scanned infected cells and moved on (shown in white tracks and **Movie S1**).

Together, these data show that T cells enter VV-infected skin and locate virus-infected cells independently of cognate Ag expression, but require antigen to stably interact with infected cells.

Infected Monocytes Produce CXCR3 Ligands In VV-Infected Skin

In order to address what factors govern $CD8^+$ T cell interactions in infected tissue, we performed chemokine and cytokine-focused qPCR arrays on mRNA isolated from uninfected or 5 day p.i. ear skin (**Figure 2**). Of 34 cytokine and β-chemokine genes examined, the four greatest increases were in interferon-γ (IFN-γ) (upregulated ~200-fold), and the β-chemokines CCL4, -7, and -20, which increased ~20-100-fold (**Figure 2A**, right panel). Even greater changes were found in the 8 α-chemokine genes tested, two of which, CXCL9 and CXCL10, demonstrated >1000-fold increases. (**Figure 2B**). Fine kinetic examination of CXCL9 and -10 expression revealed parallel increases on day 3 (**Figure 2C**), with CXCL10 mRNA peaking on day 5 (concurrent with maximal numbers of infected monocytes (**Figure S2**)) and CXCL9 mRNA peaking 2 days later.

We next sorted both infected and uninfected inflammatory monocytes from VV-infected skin (ears) on day 5 p.i based on VV-encoded GFP expression and cell surface antibody-staining ($CD45^+$ $Ly6C^+$ $CD11b^+$ cells), and analyzed α-chemokine mRNA expression (**Figure 2D**). Compared to uninfected total ear cells (in the absence of infection there are too few monocytes to isolate as a control population), both infected and uninfected inflammatory monocytes displayed increased chemokine mRNA, with infected cells demonstrating much greater (nearly 5000-fold) increases. The pattern was identical to that seen in the whole ear (the sole exception being a slight increase in CXCL1 in isolated

monocytes not observed in the whole-ear sample), consistent with inflammatory monocytes as a principal source of VV-induced chemokines. Note that the increase in infected *vs.* uninfected inflammatory monocytes demonstrates that chemokine mRNA expression was induced by VV-infection, and is not a general feature of this cell type *in situ* or an artifact of their isolation from the ear.

To confirm chemokine synthesis, we performed flow cytometric (**Figure S3**) and microscopic analyses of infected ears (**Figure 2E**). Confocal images of frozen sections of VV-infected ears taken at 5 days p.i. showed OT-I $CD8^+$ T cells (red) interacting with VV-infected (green) $CD11b^+$ (blue) cells (inflammatory monocytes). Notably, many infected cells were synthesizing CXCL9, as indicated by staining in white.

Taken together, our findings indicate that CXLC9 and 10 mRNAs are highly upregulated in VV-infected skin, and that these chemokines are abundantly expressed by infected inflammatory monocytes.

VV Infection is Exacerbated in *Cxcr3*$^{-/-}$ Mice

To understand the role of CXCL9 and -10 in the recognition of VV infected-cells *in vivo*, we infected mice deficient in CXCR3, the common receptor for these chemokines (Cole et al., 1998; Mahalingam et al., 1999). Five days p.i., we performed confocal imaging, scanning large areas of infected skin for hematopoietic cells ($CD45^+$ cells (blue) and virus-infected cells (green)) (**Figure 3A**). As previously described for wild-type (WT) mice, we identified only a small focus of remaining virus-infected cells (upper middle of left panel). In contrast, *Cxcr3*$^{-/-}$ mice infected in parallel exhibited enormous numbers of virus-infected cells throughout the ear (right panel). Immunohistochemical staining of ears for CD11b (white) revealed that the majority of infected cells were likely inflammatory monocytes (**Figure 3B**).

We next performed flow cytometric analysis of cells from enzymatically-dissociated ears to better identify and enumerate infected cell populations (**Figure 3C**). As previously described (Hickman et al., 2013), WT mice exhibit infiltration of inflammatory monocytes at 5 days p.i., many of which are infected (GFP^+) (**Figure 3C**, top panels). Cellular infiltration was remarkably similar in *Cxcr3*$^{-/-}$ mice on day 5 p.i., with equivalent numbers of inflammatory monocytes (**Figure 3B,** bottom panels and **3C**). As in WT mice, a majority of infected cells were $LY6CG^{int}$ inflammatory monocytes (**Figure 3C,** far right panels and **3F**). While the total number of inflammatory monocytes was the same at 5 days p.i., the number on day 6 was higher in *Cxcr3*$^{-/-}$ mice. Most importantly, infected inflammatory monocytes were ~ 4-fold more numerous in *Cxcr3*$^{-/-}$ mice at 5 d.p.i. (peaking at $\sim 7 \times 10^4$ infected monocytes/ear) and remained elevated until day 8 p.i. (**Figure 3E**). In parallel, *Cxcr3*$^{-/-}$ mice demonstrated increased peak VV titers, and likely delayed complete clearance (**Figure 3F**).

To determine the cell type responsible for eliminating the virus-infected inflammatory monocytes, we performed antibody-based depletions in WT or *Cxcr3*$^{-/-}$ mice (giving antibody on days 4 and 5 p.i.), then examined ears for the number of infected cells remaining on day 6 post-infection (a time when WT mice have mostly eliminated infected

cells under normal conditions) (**Figure 3G**). As previously reported (Hickman et al., 2013), depletion of $CD8^+$ T cells (but not NK cells) reduced clearance in WT mice (**Figure 3G,** middle blue bars). $CD8^+$ T cell depletion augmented by 4.5-fold the already increased numbers of inflammatory monocytes in *Cxcr3*$^{-/-}$ mice relative to depleted WT mice (green bars).

Together, these data demonstrate that CXCR3 genetic deletion delays $CD8^+$ T cell control of VV-infected inflammatory monocytes, consistent with an important role for CXCL9-10 in controlling local VV infection.

VV-Infected *Cxcr3*$^{-/-}$ Mice Exhibit Normal T Cell Activation and Skin Homing

Cxcr3$^{-/-}$ $CD4^+$ OT-II TCR transgenic T cells exhibit defective activation when transferred into WT hosts (Groom et al., 2012). To address whether a similar failure might account for the inability of *Cxcr3*$^{-/-}$ $CD8^+$ T cells to eliminate infected inflammatory monocytes, we generated homozygous *Cxcr3*$^{-/-}$ OT-I T cell receptor transgenic mice and adoptively transferred 2.5×10^5 WT or *Cxcr3*$^{-/-}$ OT-I $CD8^+$ T cells into WT recipients. Two days following infection with SIINFEKL-expressing VV, we removed draining LNs and restimulated liberated cells with synthetic SIINFEKL peptide (**Figure 4AB**). While restimulation with irrelevant peptide yielded background IFN-γ production, both *Cxcr3*$^{-/-}$ and WT cells produced high and equivalent amounts of IFN-γ in response to SIINFEKL re-stimulation (based on mean fluorescent intensity of positive cells) (**Figure 4B**). Similarly, CXCR3 genetic deficiency did not affect OT-I cells' synthesis of granzyme B (**Figure 4C**). Accordingly, *Cxcr3*$^{-/-}$ OT-I $CD8^+$ OT-I cells properly homed to the peripheral interfollicular regions of the lymph node (**Figure 4D**), the area in which direct priming occurs in the LN after VV infection (Hickman et al., 2008). Together, these data show that CXCR3 is not required for SIINFEKL-expressing VV-induced activation of OTI $CD8^+$ T cells *in vivo.*

CXCR3 can control T cell homing during both infection and autoimmunity (reviewed in (Groom and Luster, 2011a, b)). Comparing ear-immigrant T cells in WT *vs.* *Cxcr3*$^{-/-}$ mice revealed non-statistically significant changes in T cell recruitment (as a percent of total cellular recruitment) on day 6 or 7 p.i. (**Figure 4EF**). Ear-derived polyclonal *Cxcr3*$^{-/-}$ $CD8^+$ T cells synthesized IFN-γ in response to restimulation with VV-infected cells or VV-derived peptides (**Figure 4F**), with numbers of IFN-γ^+ $CD8^+$ T cells being similar on day 6 or 7 p.i. *Cxcr3*$^{-/-}$ T cell responses were actually enhanced on day 6 p.i. for B8R (the immunodominant VV determinant in C57BL/6 mice (Tscharke et al., 2005)).

Based on these findings we conclude that *Cxcr3*$^{-/-}$ $CD8^+$ T cells exhibit normal activation, tissue homing and effector cytokine secretion in response to peripheral VV infection.

Cxcr3$^{-/-}$ $CD8^+$ T Cells Fail To Efficiently Engage And Remain In Contact With Virus-Infected Cells In The Tissue

We next assessed the contribution of CXCR3 to $CD8^+$ T cell localization and killing of virus-infected cells. Prior to infection, we co-transferred WT (cyan) and *Cxcr3*$^{-/-}$ (red) OT-I $CD8^+$ T cells into WT mice. Five days p.i., we imaged ears infected with VV-NP-S-eGFP

(green) (**Figure 5**). Via MPM, we clearly visualized *Cxcr3*$^{-/-}$ CD8^{+} T cells in the dermis (distinguished by the presence of dermal collagen, **Movie S2**), consistent with *ex vivo* flow cytometric analyses showing *Cxcr3*$^{-/-}$ T cell entry into the ear. Like WT cells, *Cxcr3*$^{-/-}$ OT-I CD8^{+} T cells facilely migrated to surround large, VV-infected keratinocytic foci (**Figure 5A** and **Movie S3)**.

Since CD8^{+} T cell killing of VV-infected inflammatory monocytes contributes to poxvirus clearance in the skin (Hickman et al., 2013), we next assessed the ability of WT (cyan) or *Cxcr3*$^{-/-}$ (red) OT-I cells to locate infected cells (**Figure 5B**). Both cells located VV-infected cells (previously identified as inflammatory monocytes (Hickman et al., 2013)) outlying major keratinocytic lesions (**Movie S4**). Indeed, we occasionally visualized *Cxcr3*$^{-/-}$ T cells actively pursuing virus-infected cells (**Movie S5**). Overall, however, while high numbers of WT T cells entered fields of virus-infected cells, *Cxcr3*$^{-/-}$ T cells hesitated at the perimeter of heavily infected areas of the tissue (**Figure 5C** and **Movie S6**). To quantitate this phenomenon, we acquired MPM images of dense areas of infected monocytes (while blinded to the presence of WT cells) and quantified the percentage of WT or *Cxcr3*$^{-/-}$ OT-I cells that had entered areas of infection versus those remaining outside (**Figure 5D**). Although WT and *Cxcr3*$^{-/-}$ T cells were equally distributed outside of infected areas of the dermis, a higher percentage of WT T cells penetrated virus infected-areas compared to *Cxcr3*$^{-/-}$ T cells (**Figure 5D**).

We next used MPM to simultaneously track WT (cyan) and *Cxcr3*$^{-/-}$ (red) OT-I CD8^{+} T cells on day 5 p.i. (**Figure 5E-H**). Over 30 min imaging sessions, *Cxcr3*$^{-/-}$ OT-I CD8^{+} T cells clearly moved faster than WT cells (**Figure 5E-F** and **Movie S7**). Overlaid tracks of individual cells acquired in the same field of infected cells likewise revealed greater movement of *Cxcr3*$^{-/-}$ T cells (**Figure 5E**, left panel) than WT cells (right panel), a feature reflected in average cell speeds over the course of multiple imaging experiments (**Figure 5F**). On average, WT T cells were > 0.5 μm/min slower than *Cxcr3*$^{-/-}$ T cells (**Figure 5F**, left and middle panels). Similar to *Cxcr3*$^{-/-}$ CD4^{+} T cells interacting with antigen-pulsed APCs in the LN (Groom et al., 2012), a significantly higher proportion of *Cxcr3*$^{-/-}$ CD8^{+} T cells present in areas of intense VV infection were highly motile (25.9 % vs. 16.4 %) (**Figure 5F**, right panel).

To determine if differences in contact with infected cells could account for motility differences, we imaged WT and *Cxcr3*$^{-/-}$ OT-I cells interacting with virus-infected cells in the same field, carefully selecting a time period on day 5 p.i. for imaging that was late enough for some *Cxcr3*$^{-/-}$ T cells to penetrate infected areas, yet before all of the infected cells were lysed. While many WT OT-I cells contacted infected cells and maintained contact over 30-60 min. imaging periods, *Cxcr3*$^{-/-}$ OT-I cells were typically more mobile, moving from one infected cell to another (**Figure 5G** and **Movie S7**). To quantify this, we calculated the percentage of time that a T cell contacted an infected cell during a 1 hr. imaging period ((**Figure 5H**), note: we did not include any cells that did not stably contact an infected cell within the first 15 min. of imaging.) WT T cells remained engaged with virus-infected cells for a longer period after initiating contact (89.3 ± 2.9% (WT) vs. 61.2 ± 4.2% (*Cxcr3*$^{-/-}$) of the imaging period. Likewise, although both T cell types rapidly scanned virus-infected cells

with which they were engaged; the difference in contact times was reflected in longer pauses (*e.g.* the cell's time with an instantaneous velocity < 1 μm/min) for WT T cells (WT = 63.9 ± 3.5%; *Cxcr3*$^{-/-}$ = 36.6 ± 3%) (**Figure 5H and Figure S4**).

Taken together, these data show that relative to WT, *Cxcr3*$^{-/-}$ CD8^{+} T cells exhibit decreased presence in virus-infected regions and shorter contacts with infected cells.

Cxcr3$^{-/-}$ CD8^{+} T Cells Eliminate Virus-Infected Cells Less Efficiently

To assess the antiviral function of *Cxcr3*$^{-/-}$ *vs.* WT OT-I CD8^{+} T cells, we transferred 2.5 × 10^{5} of either cell type into WT mice, infected with VV, and analyzed cells for the production of IFN-γ at 5.5 days p.i. (**Figure 6A-D**). While the number of transferred T cells in tissues was similar in both cases (underscoring the proper homing of activated T cells lacking CXCR3 (**Figure 6A**)), direct *ex vivo* analysis (*i.e.* without restimulation) revealed the number of *Cxcr3*$^{-/-}$ OT-I cells producing IFN-γ was reduced compared to WT OT-I T cells (**Figure 6 B-C**). On a per cell basis, *Cxcr3*$^{-/-}$ and WT OT-I cells synthesized equivalent amounts of IFN-γ, reinforcing the conclusion that CXCR3 expression is not required for CD8^{+} T cell effector function, if the cells have appropriately engaged virus-infected targets (**Figure 6D**).

We further assessed the ability of *Cxcr3*$^{-/-}$ OT-I cells to control virus infection *in vivo*, by transferring *Cxcr3*$^{-/-}$ or WT OT-I cells into CD8-deficient animals and analyzing their ability to eliminate virus-infected cells using flow cytometry of cell populations from dissociated ears (**Figure 6E**). *Cxcr3*$^{-/-}$ OT-I cells clearly killed fewer infected cells than WT OT-I cells.

To more systematically examine this phenomenon and precisely control for number of T cells present in infected tissue, we titrated the number of OT-I cells transferred (ranging from 2.5 × 10^{3} to 7.5 × 10^{5} per animal) and enumerated both T cells and virus-infected cells in each infected ear (**Figure 6F-J**). This enabled us to compare pairs of animals with equivalent numbers of T cells in their ears. For each mouse pair, WT OT-I T cells (blue area fill) eliminated more infected cells than *Cxcr3*$^{-/-}$ OT-I cells (green fill) (**Figure 6F**). Over the entire range of adoptively transferred T cells used in Figure 6F, an almost identical number of either WT or *Cxcr3*$^{-/-}$ OT-I cells were present per ear (**Figure 6G**). Averaging the paired data revealed that WT cells were 4-fold more efficient at eliminating virus-infected cells (**Figure 6H-I**). Finally, WT OT-I cells significantly reduced viral titers when present in equivocal numbers as *Cxcr3*$^{-/-}$ T cells.

These data strongly indicate that *Cxcr3*$^{-/-}$ OT-I cells have a compromised ability to eliminate VV-infected cells.

Wild-type CD8^{+} T cells control enhanced VV infection of CXCR3$^{-/-}$ mice

Although our findings clearly point to an important function for CXCR3 on T cells during the clearance of virus-infected tissues, it is possible that CXCR3 expression by other cells (innate leukocytes, keratinocytes, etc.) contributes to virus clearance under normal conditions. To address this important issue, we transferred WT or *Cxcr3*$^{-/-}$ OT-I cells into *Cxcr3*$^{-/-}$ mice prior to infection with VV-NP-S-GFP, and examined infected ears on day 5

p.i. Both WT and *Cxcr3*$^{-/-}$ OT-I cells efficiently homed to infected *Cxcr3*$^{-/-}$ ears (dsRed^{+} cells, (**Figure 7A-B**)). Despite nearly equivalent entry, *Cxcr3*$^{-/-}$ ears with WT *vs.* *Cxcr3*$^{-/-}$ OT-I cells had far fewer infected inflammatory monocytes reflected in diminished viral titers (**Figure 7C-D**). Confocal tilescan imaging of frozen sections of ears confirmed the absence of large numbers of VV-infected inflammatory monocytes in mice that received WT T cells (**Figure 7E**), which now phenocopied infected tissue in WT mice (see **Figure 3A**). Conversely, confocal tilescans from *Cxcr3*$^{-/-}$ animals that received *Cxcr3*$^{-/-}$ OT-I cells more closely mirrored *Cxcr3*$^{-/-}$ animals without T cell transfer (see **Figure 3A**).

Based on these data, we conclude that the positive effects of CXCR3 expression on CD8^{+} T cell anti-viral activity can be largely if not completely ascribed to its function on CD8^{+} T cells themselves.

DISCUSSION

The chemokine receptor CXCR3 and its ligands play important roles in antiviral immunity. Effector CD8^{+} T cells upregulate CXCR3 (a transcriptional target of *t-bet*) following infection with a variety of viruses (Taqueti et al., 2006). As a G-protein coupled chemotactic receptor, CXCR3 expression affects tissue recruitment of antiviral CD8^{+} T cells (for examples see (Hokeness et al., 2007; Klein et al., 2005; Lee et al., 2005; Slutter et al., 2013)). Additionally, CXCR3 signaling can modify antiviral effector CD8^{+} T cell differentiation, as the absence of CXCR3 in murine infections with lymphocytic choriomeningitis virus (LCMV), influenza A virus (IAV) or VV results in increased memory CD8^{+} T cells at the expense of short-lived effector cells (Hu et al., 2011; Kohlmeier et al., 2011; Kurachi et al., 2011). During secondary viral infections, CXCR3 expression by lymph node memory effector CD8^{+} T cells is needed for T cell trafficking to infected peripheral tissues (Kastenmuller et al., 2013; Sung et al., 2012). Additionally, CXCR3 expression allows circulating effector T cells to home to inflamed LNs (Guarda et al., 2007). No doubt this is but a partial list of the functions of CXCR3 expression on antiviral CD8^{+} T cells.

The impact of CXCR3 deficiency on viral replication and pathogenesis in mice varies with the virus studied, though here too, much remains to be learned. *Cxcr3* genetic deficiency increases susceptibility to genital herpes simplex-2 virus (HSV-2) (Thapa and Carr, 2009) and intracerebral dengue virus (Ip and Liao, 2010). Interestingly, protection in each of these models is mediated independently of CXCR3-dependent leukocyte recruitment. CXCR3 deficiency does not appear to alter the outcome of mouse infection with either LCMV (Mahalingam et al., 1999) or HSV-1 (Wickham et al., 2005). Lee *et al.* reported no affect on morbidity but delayed viral clearance in murine gammaherpesvirus 68 infected *Cxcr3*$^{-/-}$ mice (Lee et al., 2005), which they attributed to delayed T cell recruitment (although they also observed deficient *Cxcr3*$^{-/-}$ T cell lysis of target cells). Likewise, we saw no overt changes in morbidity after epicutaneous VV infection, however *Cxcr3* genetic deficiency interfered with viral clearance at intermediate times of infection (days 5-7). These data strongly imply that *Cxcr3* deletion may result in effects in other virus models that will be missed by limiting studies to mortality or weight loss as a read-out.

Here, we report that CXCR3 can affect not only T cell migration into virus-infected or inflamed tissue, but also migration within a tissue as T cells locate virus-infected targets for killing. Although this decreased ability of *Cxcr3*$^{-/-}$ CD8^{+} T cells to effectively locate and eliminate infected cells clearly contributes to exacerbated VV infection in *Cxcr3*$^{-/-}$ mice, it is likely that additional factors enhance also infection in these animals. Prior to the entry of primed T cells into the ear, *Cxcr3*$^{-/-}$ animals exhibit elevated numbers of infected cells, indicating enhanced early virus replication and/or dissemination independent of T cell control. This suggests a possible role for CXCR3 in innate immune control of early VV replication (CXCR3 is expressed on monocytes, plasmacytoid DCs, and NK cells (Koch et al., 2009)). Additionally, *Cxcr3*$^{-/-}$ mice exhibit delayed dermal wound healing in non-infectious models (Yates et al., 2008; Yates et al., 2007), which could potentially contribute to early VV spread. Whatever the case, the enhanced VV infection we find in *Cxcr3*$^{-/-}$ mice is controlled by CD8^{+} T cells and VV is cleared even in the absence of *Cxcr3*, though this is delayed compared to WT mice.

In the current study, we did not determine all of the cell types synthesizing CXCR3 ligand(s) at different times during infection, in part due to concern about the sensitivity of immunohistochemical staining for CXCL9-10 (Groom and Luster, 2011b). It will be important to better characterize producing cells in future studies. For this purpose, recently described Rex3 mice, which report CXCL9 and 10 expression with different fluorophores (Groom et al., 2012) should be quite useful. At present, however, no system is without additional interpretational complications, as non-chemokine-producing cells can bind and display functional CXCL9-10, which would not be indicated by a fluorescent reporter system (Groom and Luster, 2011b). Importantly, CXCL9 and 10 can be induced by different stimuli and therefore expressed by different repertoires of cells, which can then alter their effects on disease (Groom and Luster, 2011a, b). Further complicating matters, the timing of CXCL9 and 10 mRNA expression is not identical in VV-infected skin as CXCL9 mRNA peaks approximately two days later than CXCL10 mRNA. Thus, it is likely that different populations of cells in the skin (perhaps including non-hematopoietic cellular skin components (Huen and Wells, 2012)) produce these two CXCR3 ligands, especially at later times in infection.

Despite these unknowns, the dramatic upregulation of CXCL9-10 mRNA in infected inflammatory monocytes, confirmed by *in situ* immunohistochemical staining of frozen tissue, suggests that these cells are a major source of CXCR3-ligands. VV-infected inflammatory monocytes largely localize in densely packed areas of the dermis adjacent to foci of virus replication in keratinocytes (Hickman et al., 2013). While anatomically confined infection likely results from local virus spread in the tissue, the presence of numerous targets in close proximity greatly enhances the ability of T cells to find and clear infection. Interestingly, we did not observe Levy walk behavior as T cells were hunting virus-infected cells (Harris et al., 2012), a feature that is likely dictated by the heavy density of “prey” (rather than sparse distribution) in the skin. Our data further suggest that infected cells produce a localized gradient of CXCR3 ligands that T cells utilize for entrance into areas of infection. Future studies are required to determine the contribution to CXCR3-dependent virus clearance of serial killing by individual cells *vs.* recruitment of greater

numbers of T cells. In the latter case, this would likely increase the importance of chemokine guidance into heavily infected areas of the tissue.

The interactions and functions mediated by CXCR3 in the tissue are clearly diverse and appropriately complex. Despite this, it may yet be possible to manipulate the system for pragmatic applications. Here, we show that CXCR3 maximizes VV clearance in peripheral tissues independently of its influence on tissue immigration, which could potentially be exploited during rational vaccine design. Intriguingly, neutralization of IL-12 shortly after IAV immunization boosts the number of CXCR3-expressing memory $CD8^+$ T cells, which then afford superior protection against subsequent IAV challenge (Slutter et al., 2013). Thus, strategies are already in place to increase CXCR3-expressing $CD8^+$ T cells that might be applied during vaccination to enhance viral clearance by maximizing T cell killing.

EXPERIMENTAL PROCEDURES

Mice

Specific pathogen-free C57BL/6, B6(Cg)-Tyrc-2J/J), STOCK Tg(CAG-DsRed*MST)1Nagy/J, and *Cxcr3*$^{-/-}$ (stock # 5796) mice were obtained from The Jackson Laboratory or from Taconic Farms. STOCK Tg(CAG-DsRed*MST)1Nagy/J were crossed to OT-I TCR transgenic mice (NIAID Intramural Research Repository), and bred for homozygosity to create DsRed OT-I mice. DsRed OT-I mice were crossed with *Cxcr3*$^{-/-}$ mice to generate homozygous female *Cxcr3*$^{-/-}$ DsRed OT-I mice. OT-I TCR transgenic mice were also crossed with CFP-expressing mice (B6.129(ICR)-Tg(CAG-ECFP)CK6Nagy/J, stock #4218, Jackson Laboratories) to create wild-type OTI CFP mice. Six-sixteen week old female mice were used in all experiments. All mice were housed under specific pathogen-free conditions (including MNV, MPV, and MHV) ands maintained on standard rodent chow and water supplied *ad libidum*. All animal studies were approved by and performed in accordance with the NIAID ACUC.

Viruses and infections

Mice were anesthetized and infected e.c. in the ear by 5 gentle pokes with a bifurcated needle dipped in VV (stock titer ~ 1×10^8 pfu/ml) as previously described (Hickman et al., 2013). VV-NP-S-eGFP contains the $CD8^+$ T cell determinant SIINFEKL recognized by OT-I $CD8^+$ T cells ;VV-NP-eGFP is an identical virus lacking the SIINFEKL determinant. Viruses were constructed as thymidine kinase (TK) negative viruses with the recombinant insert was expressed by an early-late vaccinia promoter. Fluorescence expression reports infection rather than infectious virions released.

T cell transfers

$CD8^+$ T cells were purified by negative selection using an AutoMACS (Miltenyi Biotec). Cells were 90-95% pure by flow cytometry. 2.5×10^5 (unless dose is otherwise indicated) OT-I cells were transferred i.v. prior to infection. For some multiphoton imaging experiments, wild-type CFP-expressing OT-I cells and *Cxcr3*$^{-/-}$ dsRed-expressing OT-I cells were co-injected.

Flow cytometric analyses

Single cell suspensions of ears were prepared by collagenase digestion (Type I, Worthington Biochemicals) for 1 hr at 37°C prior to filtration through 70 m nylon cell strainers. Cells were stained with the following antibodies CD45 (clone 30-F11), CD8 (clone 53-6.7), CD11b (clone M1/70), and Ly6CG (clone Gr-1) (eBioscience). OT-I cells were identified based on CFP or dsRed expression. For intracellular staining for IFN-γ production, brefeldin A (10 g/ml, Sigma-Aldrich) was added during collagenase digestion, and cells were incubated 2 hrs in RPMI containing BFA. Cells were stained, fixed for 20 min with 1% paraformaldehyde, washed, then stained with anti-IFN-γ (clone XMG1.2) in .5% saponin overnight at 4° C. Cells we re analyzed on an LSR II flow cytometer (BD Biosciences) and data analyzed using FlowJo (Treestar).

Viral titering via plaque assay

Ears were removed at various times p.i., collagenase digested for 1 hour at 37 °C, and disrupted by vigorous pipetting. This suspension was freeze-thawed 3X, sonicated 3X, serially diluted and plated on TK^- cells. Cells were incubated for 2 d. after before counting plaques.

Ab depletion

For Ab-based depletions, 0.5 mg of either anti-CD8 Ab (clone 53-6.7) or anti-NK cell Ab (clone NK1.1) was given daily ip. beginning on day 5 post-infection (just prior to T cell entry into infected skin) as described in (Hickman et al., 2013). Ears were analyzed on day 5 and day 6 p.i.

qPCR arrays

Ears were removed and the dorsal and ventral halves were separated and immediately deposited in Trizol (Sigma). Ears were chopped into small pieces, then homogenized and passed through a 20-gauge needle. RNA was isolated according to the manufacturer's instructions, and then purified using a Qiagen RNAEasy Mini Kit (Qiagen). An on column DNAse digestion was performed prior to RNA elution. CDNA were made using the RT^2 First Strand Kit (Qiagen) starting with 2.5 g of RNA/sample. CDNA were loaded onto an Inflammatory Cytokines and Receptors qPCR array (PAMM-011Z, Qiagen), and RT-PCR data acquired on a RealPlex RT-PCR machine (Eppendorf). Rox was used as a loading control. Fold-changes of genes of interest were calculated against 5 standard housekeeping genes included on the same plate using the manufacturer's data analysis software base upon CT (SABiosciences, now Qiagen).

Statistics

Statistical significances were calculated by Graphpad (Prism) using the indicated tests. All *t* test performed were two-tailed.

Confocal microscopy of frozen sections

Ears were removed at indicated times, fixed overnight in PLP buffer, and placed in 30% sucrose-PBS for 24 hours before embedding in OCT medium (Electron Microscopy

Sciences) and freezing in dry-ice cooled isopentane. Twenty-micron sections were cut on a Leica cryostat (Leica Microsystems). Sections were blocked with 5% goat, donkey or rabbit serum, then stained with the one or more of following: CD11b (clone M1/70), B220 (clone RA3-6B2), CD45 (clone 30-F11), CXCL9 (clone MIG-2F5.5, Biolegend), keratin 10 (rabbit polyclonal, Abcam), CD69 (polyclonal goat, R&D Systems).

Intravital MPM imaging

MPM imaging was performed as described previously (Hickman et al., 2013; Hickman et al., 2008). Briefly, images were acquired on an upright Leica SP5 confocal microscope (Leica Microsystems) equipped with two Mai Tai Ti:Sapphire lasers (Spectra Physics). Ears were immobilized and bathed in warm saline. Images were acquired with a 20x dipping objective (NA 1.00). Images were obtained at 900 nm for eGFP-collagen-dsRed imaging. For imaging CFP-collagen-GFP-sRed, imaging was performed in sequential mode at 900 nm and 800 nm (for CFP excitation). Emitted fluorescence was collected with a four-channel non-descanned detector. Wavelength separation was accomplished with a 495 nm dichroic mirror followed by emission filters of 460/50 nm and 525/50 nm. The red channel was collected after a 560 nm dichroic with a 610/60 bandpass emission filter. For most movies (e.g. when time was critical), images were acquired using 2X zoom and a 3-μm Z-step for a total depth of 45 μm every 30 sec. During sequential mode, this time interval was extended to 1-3 min between series (needed to switch lasers).

MPM analysis

Maximum intensity projections processed from z-stacks using Imaris (Bitplane). To track cellular movement, images were processed using a Gaussian filter, then tracks calculated using the “spot” function. Overlaid tracks were generated using Imaris XT function “translate tracks” and pseudocolored according to the average speed of the cell creating the track. Average speeds were calculated using the following parameters: autoregressive motion, gapclose 1, 7.5 μm object diameter, 20 μm maximum distance. Created tracks were analyzed individually by hand for erroneous connections.

For analysis of the percentage of T cells that entered virus-infected areas, microscopic fields were selected based on the presence of high densities of GFP^+ non-keratinocytic infected cells. Fields were collected so that approximately 50-75% of the field contained infected cells and was blinded to the presence of wild-type T cells. WT and *Cxcr3*$^{-/-}$ T cells were enumerated using spot detection software (Imaris) inside and outside the area of infected cells. The percentage of WT or *Cxcr3*$^{-/-}$ $CD8^+$ T cells within the area of virus-infected cells (as a function of the total number of T cells present in the image) was then calculated. Data were plotted using Graphpad software (Prism).

For analysis of contact times with infected cells, it was critical to wait until day 5.5-6.0 p.i. when *Cxcr3*$^{-/-}$ T cells had time to enter areas of viral infection (yet before the infected cells were lysed). One hr movies were collected with 4 μm z-step size at 2X magnification. Tracks were created manually because the large number of cells present resulted in erroneous classifications by automated tracking. Contact time per infected cell was manually assigned for at 15-30 cells per independent experiment and reported as a percent of time in

contact during the total 1 hr imaging period. The number of “pause” steps was calculated automatically using the ImarisXT function “calculate track length” with input value of pausing of 1 μm/min.

Supplementary Material

Refer to Web version on PubMed Central for supplementary material.

ACKNOWLEDGMENTS

The authors would like to thank members of the Comparative Medicine Branch for excellence in animal husbandry, the NIAID flow cytometry facility (Bishop Hague and Elina Stregevsky) for cell sorting, and the NIAID Biological Imaging facility (Owen Schwartz) for assistance with microscopy. This work was supported by the Intramural Research Program of the NIH, NIAID.

Abbreviations

Ab	antibody
Ag	antigen
d.	day
d.p.i.	day post-infection
GFP	green fluorescent protein
HSV	herpes simplex virus
IFN-γ	interferon-gamma
LN	lymph node
LCMV	lymphocytic choriomeningitis virus
mfi	mean fluorescence intensity
MIP	maximum intensity projection
MPM	multiphoton microscopy
p.i.	post infection
SEM	standard error of the mean
TK	thymidine kinase
VV	vaccinia virus
WT	wild-type

REFERENCES

Cole KE, Strick CA, Paradis TJ, Ogborne KT, Loetscher M, Gladue RP, Lin W, Boyd JG, Moser B, Wood DE, et al. Interferon-inducible T cell alpha chemoattractant (I-TAC): a novel non-ELR CXC chemokine with potent activity on activated T cells through selective high affinity binding to CXCR3. J Exp Med. 1998; 187:2009–2021. [PubMed: 9625760]

Friedl P, Weigelin B. Interstitial leukocyte migration and immune function. Nat Immunol. 2008; 9:960–969. [PubMed: 18711433]

Gordon SN, Cecchinato V, Andresen V, Heraud JM, Hryniewicz A, Parks RW, Venzon D, Chung HK, Karpova T, McNally J, et al. Smallpox vaccine safety is dependent on T cells and not B cells. J Infect Dis. 2011; 203:1043–1053. [PubMed: 21450994]

Groom JR, Luster AD. CXCR3 in T cell function. Experimental cell research. 2011a; 317:620–631. [PubMed: 21376175]

Groom JR, Luster AD. CXCR3 ligands: redundant, collaborative and antagonistic functions. Immunol Cell Biol. 2011b; 89:207–215. [PubMed: 21221121]

Groom JR, Richmond J, Murooka TT, Sorensen EW, Sung JH, Bankert K, von Andrian UH, Moon JJ, Mempel TR, Luster AD. CXCR3 chemokine receptor-ligand interactions in the lymph node optimize CD4+ T helper 1 cell differentiation. Immunity. 2012; 37:1091–1103. [PubMed: 23123063]

Guarda G, Hons M, Soriano SF, Huang AY, Polley R, Martin-Fontecha A, Stein JV, Germain RN, Lanzavecchia A, Sallusto F. L-selectin-negative CCR7-effector and memory CD8+ T cells enter reactive lymph nodes and kill dendritic cells. Nature immunology. 2007; 8:743–752. [PubMed: 17529983]

Harris TH, Banigan EJ, Christian DA, Konradt C, Tait Wojno ED, Norose K, Wilson EH, John B, Weninger W, Luster AD, et al. Generalized Levy walks and the role of chemokines in migration of effector CD8+ T cells. Nature. 2012; 486:545–548. [PubMed: 22722867]

Henrickson SE, von Andrian UH. Single-cell dynamics of T-cell priming. Curr Opin Immunol. 2007; 19:249–258. [PubMed: 17433876]

Hickman HD, Bennink JR, Yewdell JW. From optical bench to cageside: intravital microscopy on the long road to rational vaccine design. Immunol Rev. 2011a; 239:209–220. [PubMed: 21198674]

Hickman HD, Li L, Reynoso GV, Rubin EJ, Skon CN, Mays JW, Gibbs J, Schwartz O, Bennink JR, Yewdell JW. Chemokines control naive CD8+ T cell selection of optimal lymph node antigen presenting cells. The Journal of experimental medicine. 2011b; 208:2511–2524. [PubMed: 22042976]

Hickman HD, Reynoso GV, Ngudiankama BF, Rubin EJ, Magadan JG, Cush SS, Gibbs J, Molon B, Bronte V, Bennink JR, Yewdell JW. Anatomically restricted synergistic antiviral activities of innate and adaptive immune cells in the skin. Cell Host Microbe. 2013; 13:155–168. [PubMed: 23414756]

Hickman HD, Takeda K, Skon CN, Murray FR, Hensley SE, Loomis J, Barber GN, Bennink JR, Yewdell JW. Direct priming of antiviral CD8+ T cells in the peripheral interfollicular region of lymph nodes. Nature immunology. 2008; 9:155–165. [PubMed: 18193049]

Hokeness KL, Deweerd ES, Munks MW, Lewis CA, Gladue RP, Salazar-Mather TP. CXCR3-dependent recruitment of antigen-specific T lymphocytes to the liver during murine cytomegalovirus infection. J Virol. 2007; 81:1241–1250. [PubMed: 17108043]

Hsieh MF, Lai SL, Chen JP, Sung JM, Lin YL, Wu-Hsieh BA, Gerard C, Luster A, Liao F. Both CXCR3 and CXCL10/IFN-inducible protein 10 are required for resistance to primary infection by dengue virus. Journal of immunology. 2006; 177:1855–1863.

Hu JK, Kagari T, Clingan JM, Matloubian M. Expression of chemokine receptor CXCR3 on T cells affects the balance between effector and memory CD8 T-cell generation. Proc Natl Acad Sci U S A. 2011; 108:E118–127. [PubMed: 21518913]

Huen AC, Wells A. The Beginning of the End: CXCR3 Signaling in Late-Stage Wound Healing. Adv Wound Care (New Rochelle). 2012; 1:244–248. [PubMed: 24527313]

Ip PP, Liao F. Resistance to dengue virus infection in mice is potentiated by CXCL10 and is independent of CXCL10-mediated leukocyte recruitment. Journal of immunology. 2010; 184:5705–5714.

Kastenmuller W, Brandes M, Wang Z, Herz J, Egen JG, Germain RN. Peripheral prepositioning and local CXCL9 chemokine-mediated guidance orchestrate rapid memory CD8+ T cell responses in the lymph node. Immunity. 2013; 38:502–513. [PubMed: 23352234]

Klein RS, Lin E, Zhang B, Luster AD, Tollett J, Samuel MA, Engle M, Diamond MS. Neuronal CXCL10 directs CD8+ T-cell recruitment and control of West Nile virus encephalitis. J Virol. 2005; 79:11457–11466. [PubMed: 16103196]

Koch MA, Tucker-Heard G, Perdue NR, Killebrew JR, Urdahl KB, Campbell DJ. The transcription factor T-bet controls regulatory T cell homeostasis and function during type 1 inflammation. Nature immunology. 2009; 10:595–602. [PubMed: 19412181]

Kohlmeier JE, Reiley WW, Perona-Wright G, Freeman ML, Yager EJ, Connor LM, Brincks EL, Cookenham T, Roberts AD, Burkum CE, et al. Inflammatory chemokine receptors regulate CD8(+) T cell contraction and memory generation following infection. The Journal of experimental medicine. 2011; 208:1621–1634. [PubMed: 21788409]

Kurachi M, Kurachi J, Suenaga F, Tsukui T, Abe J, Ueha S, Tomura M, Sugihara K, Takamura S, Kakimi K, Matsushima K. Chemokine receptor CXCR3 facilitates CD8(+) T cell differentiation into short-lived effector cells leading to memory degeneration. The Journal of experimental medicine. 2011; 208:1605–1620. [PubMed: 21788406]

Lammermann T, Bader BL, Monkley SJ, Worbs T, Wedlich-Soldner R, Hirsch K, Keller M, Forster R, Critchley DR, Fassler R, Sixt M. Rapid leukocyte migration by integrin-independent flowing and squeezing. Nature. 2008; 453:51–55. [PubMed: 18451854]

Lee BJ, Giannoni F, Lyon A, Yada S, Lu B, Gerard C, Sarawar SR. Role of CXCR3 in the immune response to murine gammaherpesvirus 68. Journal of virology. 2005; 79:9351–9355. [PubMed: 15994833]

Lim JK, Murphy PM. Chemokine control of West Nile virus infection. Exp Cell Res. 2011; 317:569–574. [PubMed: 21376172]

Liu L, Zhong Q, Tian T, Dubin K, Athale SK, Kupper TS. Epidermal injury and infection during poxvirus immunization is crucial for the generation of highly protective T cell-mediated immunity. Nat Med. 2010; 16:224–227. [PubMed: 20081864]

Mahalingam S, Farber JM, Karupiah G. The interferon-inducible chemokines MuMig and Crg-2 exhibit antiviral activity In vivo. Journal of virology. 1999; 73:1479–1491. [PubMed: 9882354]

Mota BE, Gallardo-Romero N, Trindade G, Keckler MS, Karem K, Carroll D, Campos MA, Vieira LQ, da Fonseca FG, Ferreira PC, et al. Adverse events post smallpox-vaccination: insights from tail scarification infection in mice with Vaccinia virus. PLoS One. 2011; 6:e18924. [PubMed: 21526210]

Mueller SN, Hickman HD. In vivo imaging of the T cell response to infection. Curr Opin Immunol. 2010; 22:293–298. [PubMed: 20080040]

Overstreet MG, Gaylo A, Angermann BR, Hughson A, Hyun YM, Lambert K, Acharya M, Billroth-Maclurg AC, Rosenberg AF, Topham DJ, et al. Inflammation-induced interstitial migration of effector CD4(+) T cells is dependent on integrin alphaV. Nat Immunol. 2013; 14:949–958. [PubMed: 23933892]

Proudfoot AE, Handel TM, Johnson Z, Lau EK, LiWang P, Clark-Lewis I, Borlat F, Wells TN, Kosco-Vilbois MH. Glycosaminoglycan binding and oligomerization are essential for the in vivo activity of certain chemokines. Proc Natl Acad Sci U S A. 2003; 100:1885–1890. [PubMed: 12571364]

Rot A. Neutrophil attractant/activation protein-1 (interleukin-8) induces in vitro neutrophil migration by haptotactic mechanism. Eur J Immunol. 1993; 23:303–306. [PubMed: 8419183]

Slutter B, Pewe LL, Kaech SM, Harty JT. Lung airway-surveilling CXCR3(hi) memory CD8(+) T cells are critical for protection against influenza A virus. Immunity. 2013; 39:939–948. [PubMed: 24238342]

Sung JH, Zhang H, Moseman EA, Alvarez D, Iannacone M, Henrickson SE, de la Torre JC, Groom JR, Luster AD, von Andrian UH. Chemokine guidance of central memory T cells is critical for antiviral recall responses in lymph nodes. Cell. 2012; 150:1249–1263. [PubMed: 22980984]

Taqueti VR, Grabie N, Colvin R, Pang H, Jarolim P, Luster AD, Glimcher LH, Lichtman AH. T-bet controls pathogenicity of CTLs in the heart by separable effects on migration and effector activity. Journal of immunology. 2006; 177:5890–5901.

Thapa M, Carr DJ. CXCR3 deficiency increases susceptibility to genital herpes simplex virus type 2 infection: Uncoupling of CD8+ T-cell effector function but not migration. Journal of virology. 2009; 83:9486–9501. [PubMed: 19587047]

Tscharke DC, Karupiah G, Zhou J, Palmore T, Irvine KR, Haeryfar SM, Williams S, Sidney J, Sette A, Bennink JR, Yewdell JW. Identification of poxvirus CD8+ T cell determinants to enable rational

design and characterization of smallpox vaccines. The Journal of experimental medicine. 2005; 201:95–104. [PubMed: 15623576]

Wickham S, Lu B, Ash J, Carr DJ. Chemokine receptor deficiency is associated with increased chemokine expression in the peripheral and central nervous systems and increased resistance to herpetic encephalitis. J Neuroimmunol. 2005; 162:51–59. [PubMed: 15833359]

Yates CC, Whaley D, A YC, Kulesekaran P, Hebda PA, Wells A. ELR-negative CXC chemokine CXCL11 (IP-9/I-TAC) facilitates dermal and epidermal maturation during wound repair. Am J Pathol. 2008; 173:643–652. [PubMed: 18669615]

Yates CC, Whaley D, Kulasekeran P, Hancock WW, Lu B, Bodnar R, Newsome J, Hebda PA, Wells A. Delayed and deficient dermal maturation in mice lacking the CXCR3 ELR-negative CXC chemokine receptor. Am J Pathol. 2007; 171:484–495. [PubMed: 17600132]

HIGHLIGHTS

- CXCR3 ligands are upregulated in VV-infected skin
- *Cxcr3*$^{-/-}$ mice have normal T cell numbers in infected skin but enhanced infection
- *Cxcr3*$^{-/-}$ T cells are defective in locating virus-infected cells for killing *in situ*
- Transfer of wild-type CD8^{+} T cells restores viral control in *Cxcr3*$^{-/-}$ animals

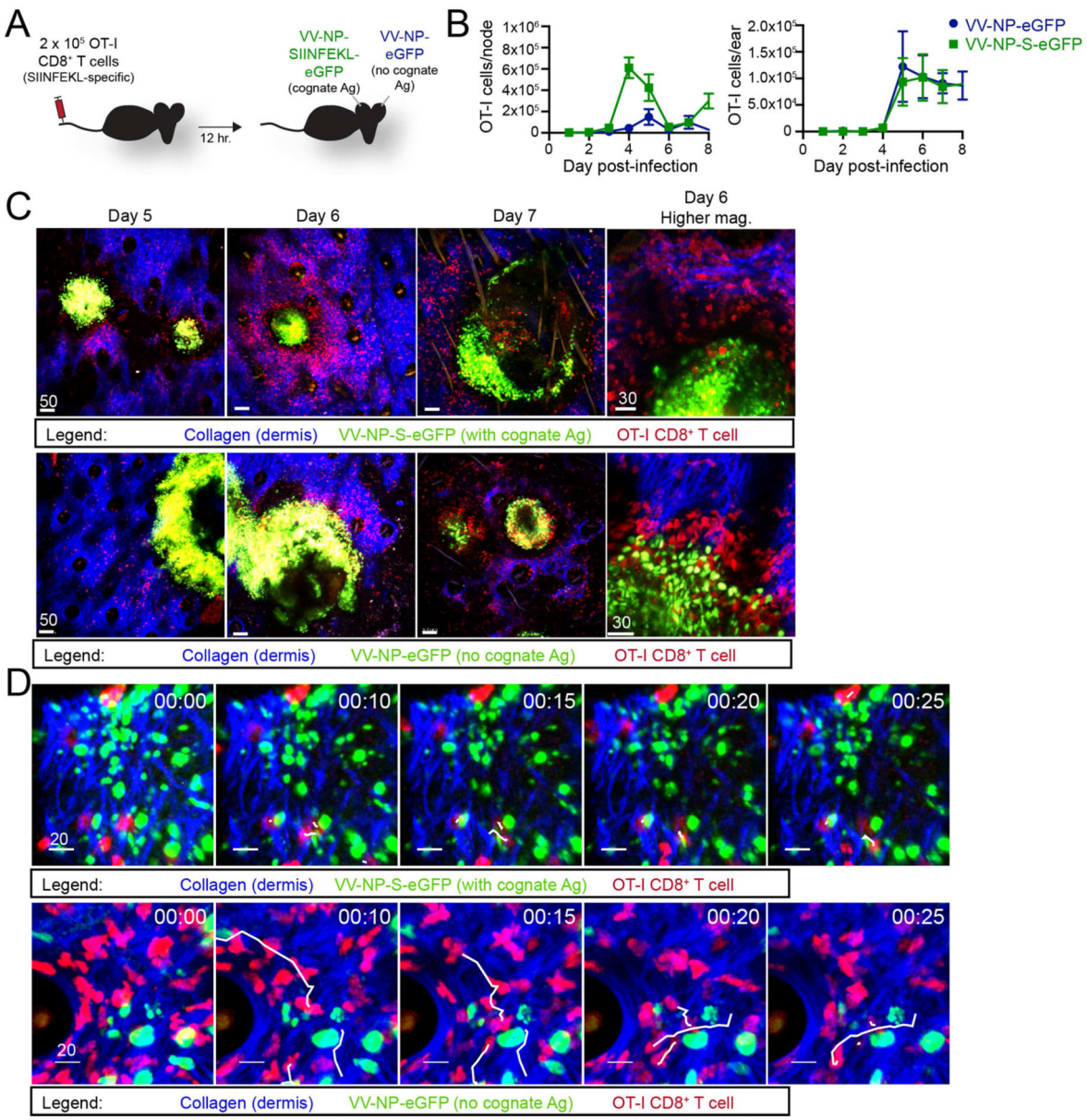

Figure 1. CD8$^+$ T cells find virus-infected cells that don't express cognate antigen

A. Experimental design. 2.5 × 10^5 OT-I T cells were transferred into wild-type (WT) animals prior to epicutaneous (ec.) infection in one ear with VV-NP-S-eGFP (with cognate Ag) and in the contralateral ear with NP-eGFP (no cognate Ag). **B**. OT-I cells per node (left) or ear (right) as determined by flow cytometric analysis. Infection with NP-S-eGFP (green); NP-e (blue). Time p.i. (days) = x axis. Error bars = SEM for 3-5 mice per group/timepoint. **C**. Maximum intensity projections (MIPs) of multiphoton microscopic (MPM) images of VV-infected ears taken at indicated day p.i. (top of images). Dermal collagen (blue); OT-I CD8$^+$ T cells (red); virus-infected cells (green). Top panels = virus expressing SIINFEKL; bottom panels lacking SIINFEKL. Higher magnification images on day 6 p.i. (far right). **D**. Time-lapse MIP MPM images from day 5 p.i. with a contralateral infection as described in A. White lines = paths of selected CD8$^+$ T cells during the 25 min. imaging period. Time

(upper right hand) = min. All experiments were repeated 3 times with 3-5 mice/group. All scalebars = microns. See also Figure S1 and Movie S1.

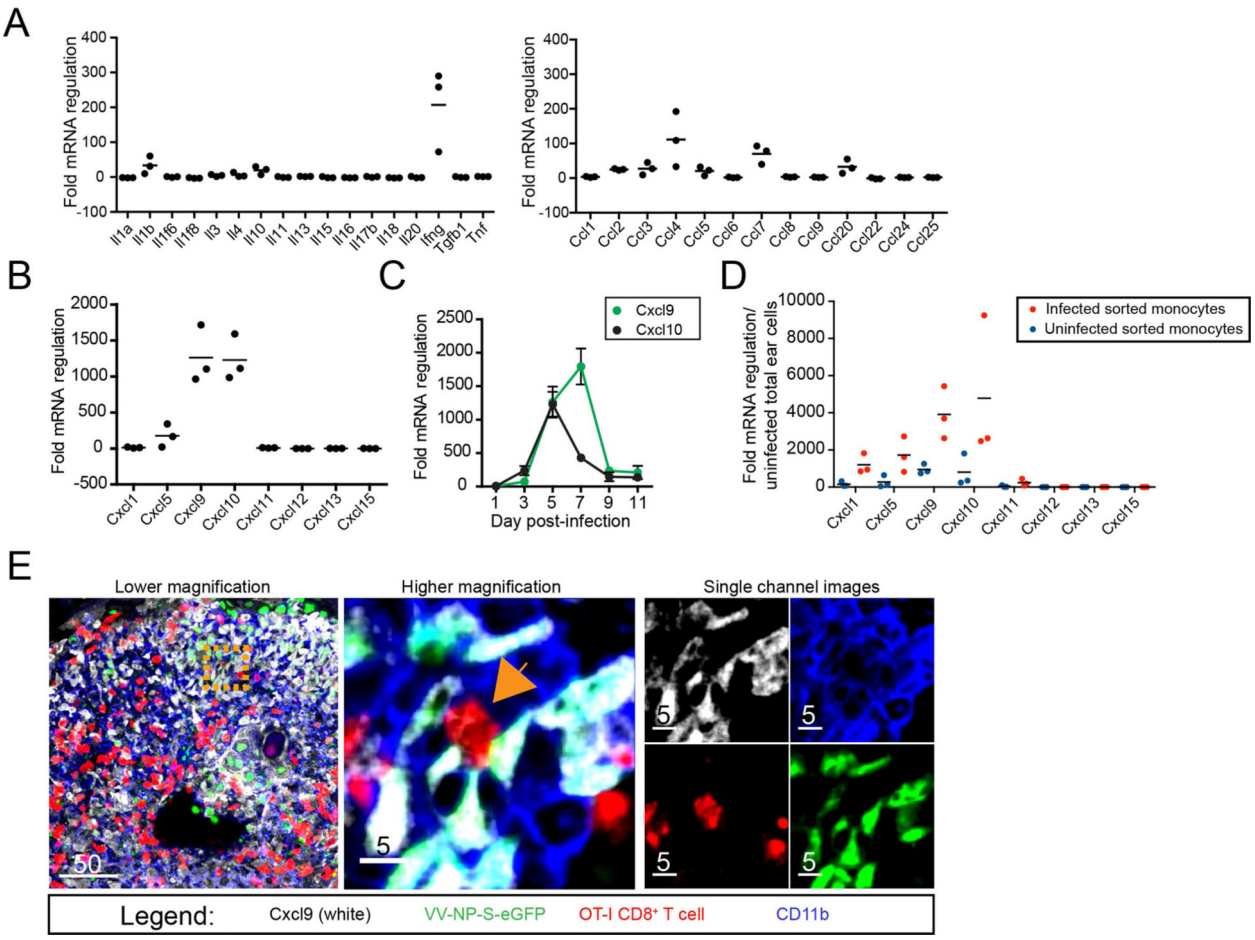

Figure 2. CXCR3 ligands are upregulated in VV-infected skin

A. Fold regulation of mRNA in VV-infected ears 5 days p.i. compared to uninfected ears. Black lines = means. **B.** as in A. but showing α-chemokine mRNA changes. **C**. CXCL9 (green) and CXCL10 (blue) mRNA expression in infected skin at indicated day p.i. (x axis) **D**. Fold regulation of mRNA in uninfected (blue dots) or infected (red dots) inflammatory monocytes sorted from day 5 infected ears. **E**. Confocal images of frozen tissue sections 5 days p.i. with VV-NP-S-eGFP (green nuclear staining), CXCL9 (white), OT-I T cells (red) and CD11b (blue). Middle panel = higher magnification of orange dashed square from left panel. Orange arrow indicates an OT-I $CD8^+$ T cell that is interacting with VV-infected $CXCL9^+$ $CD11b^+$ cells. Right panels = images of middle panel showing only one color (channel) for clarity. Scalebars = microns. All experiments were repeated 3 times. For mRNA data, dots = separate experiments with 2-5 mice/group. See also Figures S2 and S3.

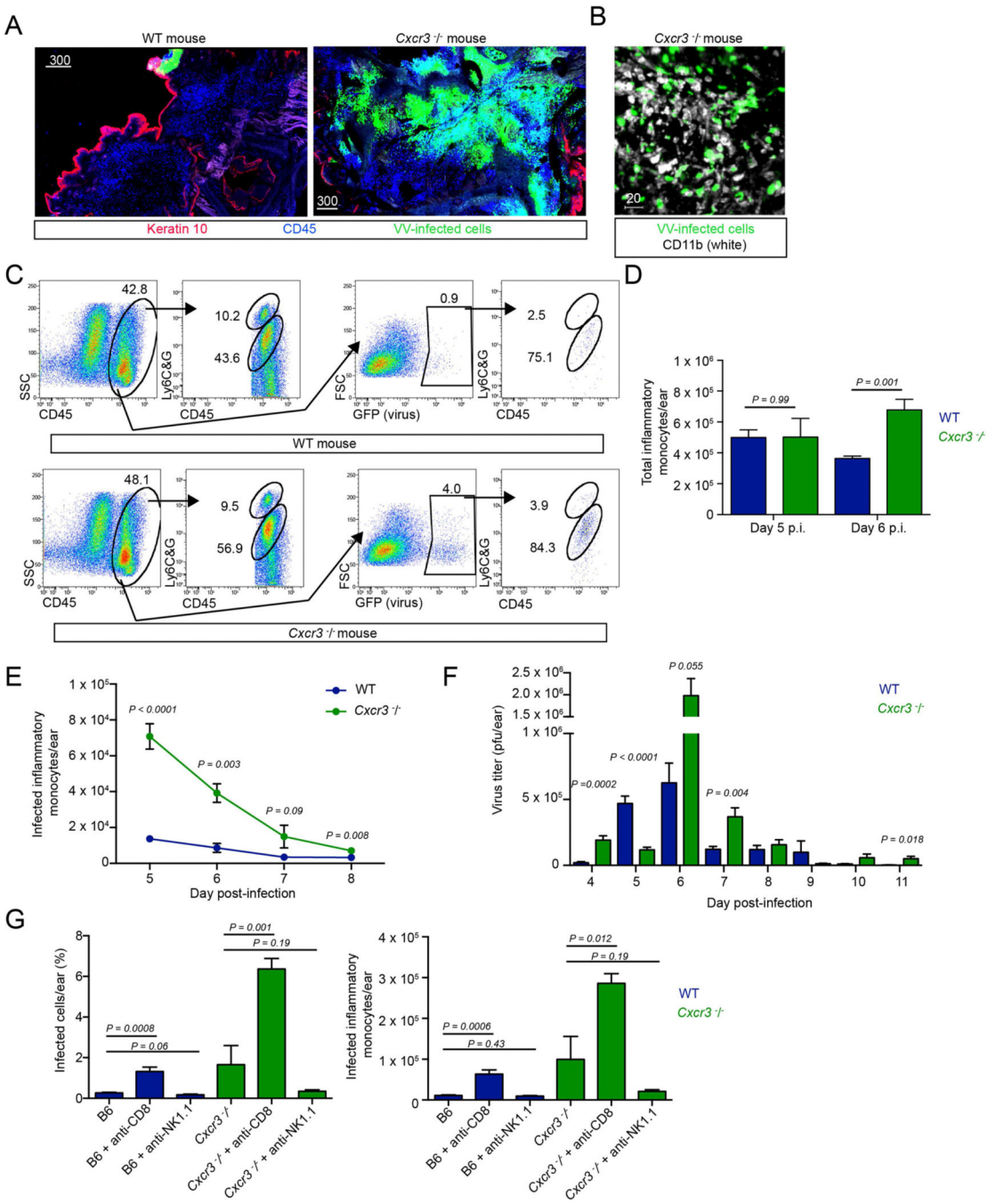

Figure 3. *Cxcr3*$^{-/-}$ mice have elevated numbers of VV-infected inflammatory monocytes

A. Confocal montages of frozen sections of WT (left) or *Cxcr3*$^{-/-}$ ears 5 days p.i. (right). VV-infected cells (green), keratin 10 (red), CD45 (blue). **B**. Confocal image of *Cxcr3*$^{-/-}$ ear 5 days p.i. CD11b (white), VV-infected cells (green). **C**. Flow histograms from dissociated ear 5 days p.i. Top panels = wild-type (WT). Bottom panels = *Cxcr3*$^{-/-}$. Middle left dot plots in both WT and *Cxcr3*$^{-/-}$ mice are gated on total cells. Middle right dot plots show infected (GFP^{+}) cells. Far right dot plots are gated on infected cells and show the percentage of infected cells that are inflammatory monocytes (Ly6CG intermediate cells) and infected

neutrophils (Ly6CG high cells). **D.** Total inflammatory monocytes on days 5-6 p.i. in WT (blue) or *Cxcr3*$^{-/-}$ (green) ears. **E.** Timecourse of infected inflammatory monocytes in WT (blue) or *Cxcr3*$^{-/-}$ (green) ears. **F**. Titer of infectious virus recovered per ear on day 5 or 6 p.i. WT (blue), *Cxcr3*$^{-/-}$ (green). **G.** Percentage and number of infected inflammatory monocytes in WT (blue) or *Cxcr3*$^{-/-}$ ears (green) day 6 p.i. Ab treatment group (performed prior to T cell entrance into the ear on days 4 and 5 p.i.) = x axis. Scalebars = microns. Error bars = SEM. Statistics = unpaired *t* tests. All experiments were repeated at least 3 times with 2-5 mice/group

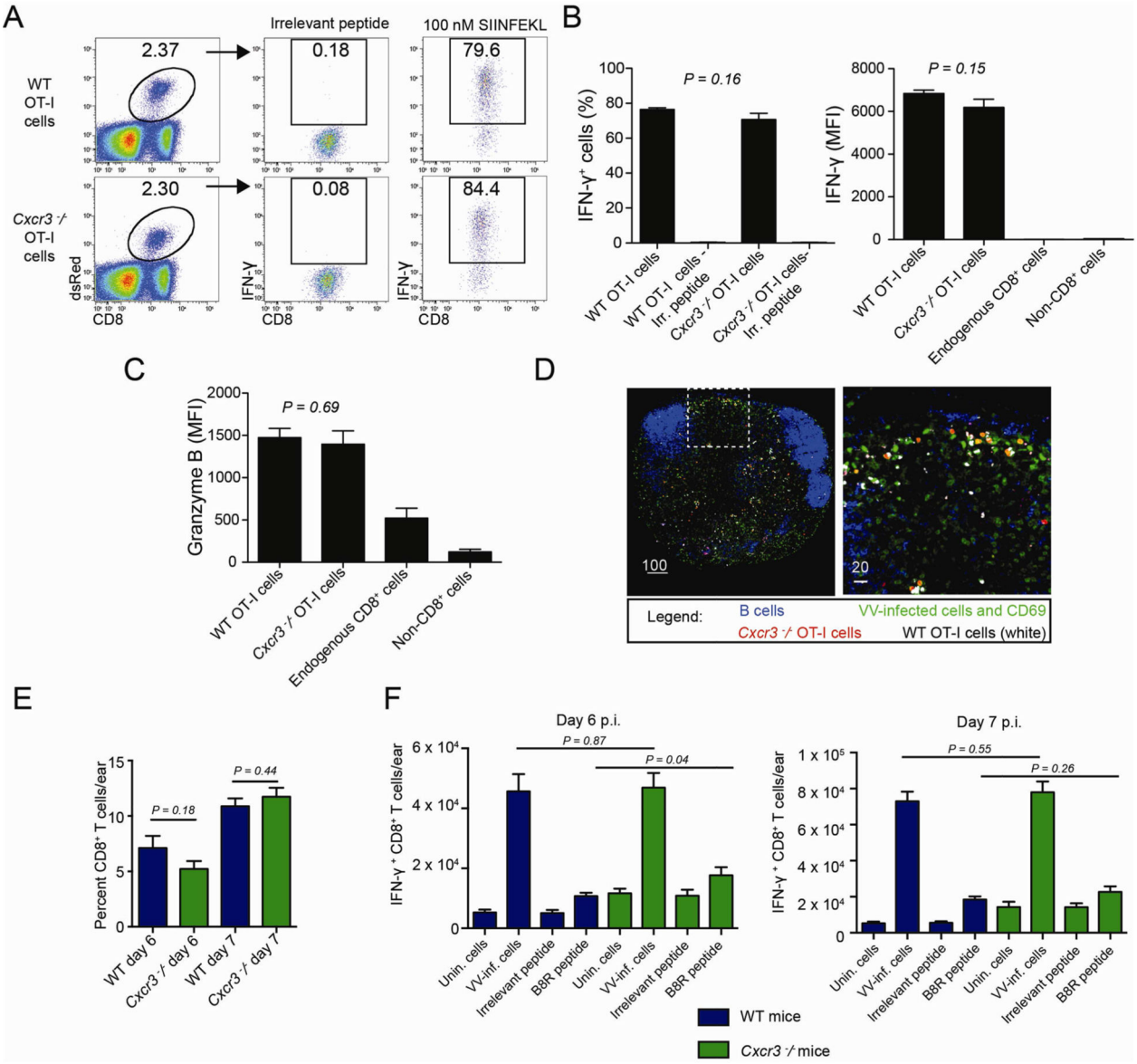

Figure 4. *Cxcr3*$^{-/-}$ CD8^{+} T cells activate and home normally

A. Dot plots from lymph node cells 2 days p.i. with VV-NP-S-eGFP. Mice were given 2.5 × 10^5 WT or *Cxcr3*$^{-/-}$ OT-I CD8^{+} T cells prior to infection. Gates show percentage of IFN-γ^{+} cells after restimulation with indicated peptide (top). **B.** Percentage (left) and MFI (right) of IFN-γ^{+} cells after restimulation. Endogenous CD8^{+} cells (all non-transferred CD8^{+} T cells in the lymph node) are shown for comparison. **C.** MFI of granzyme B. **D.** Frozen lymph node section 8 hr. p.i. with VV (green), B cells (blue), WT (white) or *Cxcr3*$^{-/-}$ (red) OT-I CD8^{+} T cells. CD69 is also stained green to indicate activated cells**. E.** Number of endogenous CD8^{+} T cells per ear days 6-7 p.i. WT = blue lines, *Cxcr3*$^{-/-}$ = green lines. **F.** Number of IFN-γ^{+} cells per ear in WT (blue) or *Cxcr3*$^{-/-}$ (green) mice on days 6 (left panel) or 7 (right panel) pi. Scalebars = microns. Error bars = SEM. Statistics = unpaired *t* tests. All experiments were repeated at least 3 times with 4-6 mice/group.

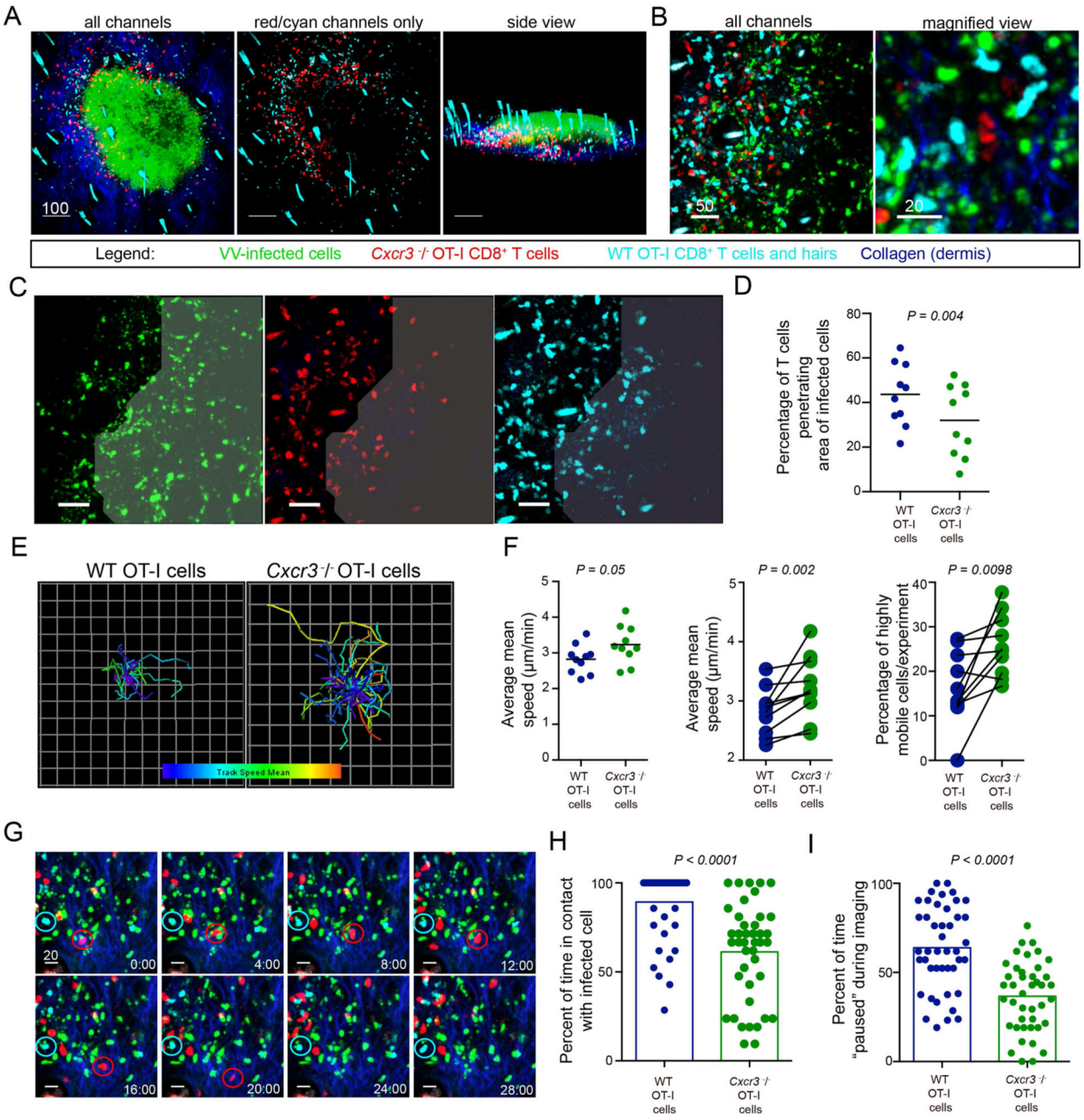

Figure 5. *Cxcr3*$^{-/-}$ CD8^{+} T cells have reduced entry into areas of infection and fail to efficiently contact virus-infected cells

A. MPM images of skin 5 days p.i. with VV (green), dermis (blue), WT (cyan) or *Cxcr3*$^{-/-}$ (red) OT-I CD8^{+} T cells. Note that autofluorescent hairs also appear cyan. **B.** MPM images from an area with many infected inflammatory monocytes (green). **C.** MPM images showing distribution of WT (cyan) or *Cxcr3*$^{-/-}$ (red) OT-I CD8^{+} T cells within a densely infected area (indicated by shading). For clarity, each color is shown independently. **D.** Percentage of WT (blue) or *Cxcr3*$^{-/-}$ (green) OT-I CD8^{+} T cells within densely infected areas. Dots represent individual microscopic fields. Line = mean. **E.** Overlaid tracks of T cells from the same field during a 30 min. imaging period. Tracks are color-coded from slow

(blue) to fast (red). **F.** Average mean speeds of WT (blue) or *Cxcr3*$^{-/-}$ (green) OT-I CD8^{+} T cells from same field in an imaging session (left panel, statistics = Mann Whitney test). Middle panel = WT or *Cxcr3*$^{-/-}$ OT-I T cells in same field connected with a line (statistics = Wilcoxon test). Right panel shows percentage of cells moving > 2 SDs from mean speed of WT OT-I CD8^{+} T cells with lines indicating pairs in same imaging field (statistics = Wilcoxon test). **G**. Still frame MPM images of WT (cyan) or *Cxcr3*$^{-/-}$ (red) OT-I T cells over 30 min.. A WT cell (cyan circle) and a *Cxcr3*$^{-/-}$ cell (red circle) is followed over time. **H.** (Left) Percent of time WT (blue) and *Cxcr3*$^{-/-}$ (green) cells are contacting infected cells during 1 hr. imaging period. (Right) Percent of time paused on infected cell. Results were combined from two individual experiments and repeated twice. Time = min. Scalebars = microns. Error bars = SEM. All experiments except **H** were repeated at least 3 times with 4-6 mice/group. See also Figure S4 and Movies S2-S7.

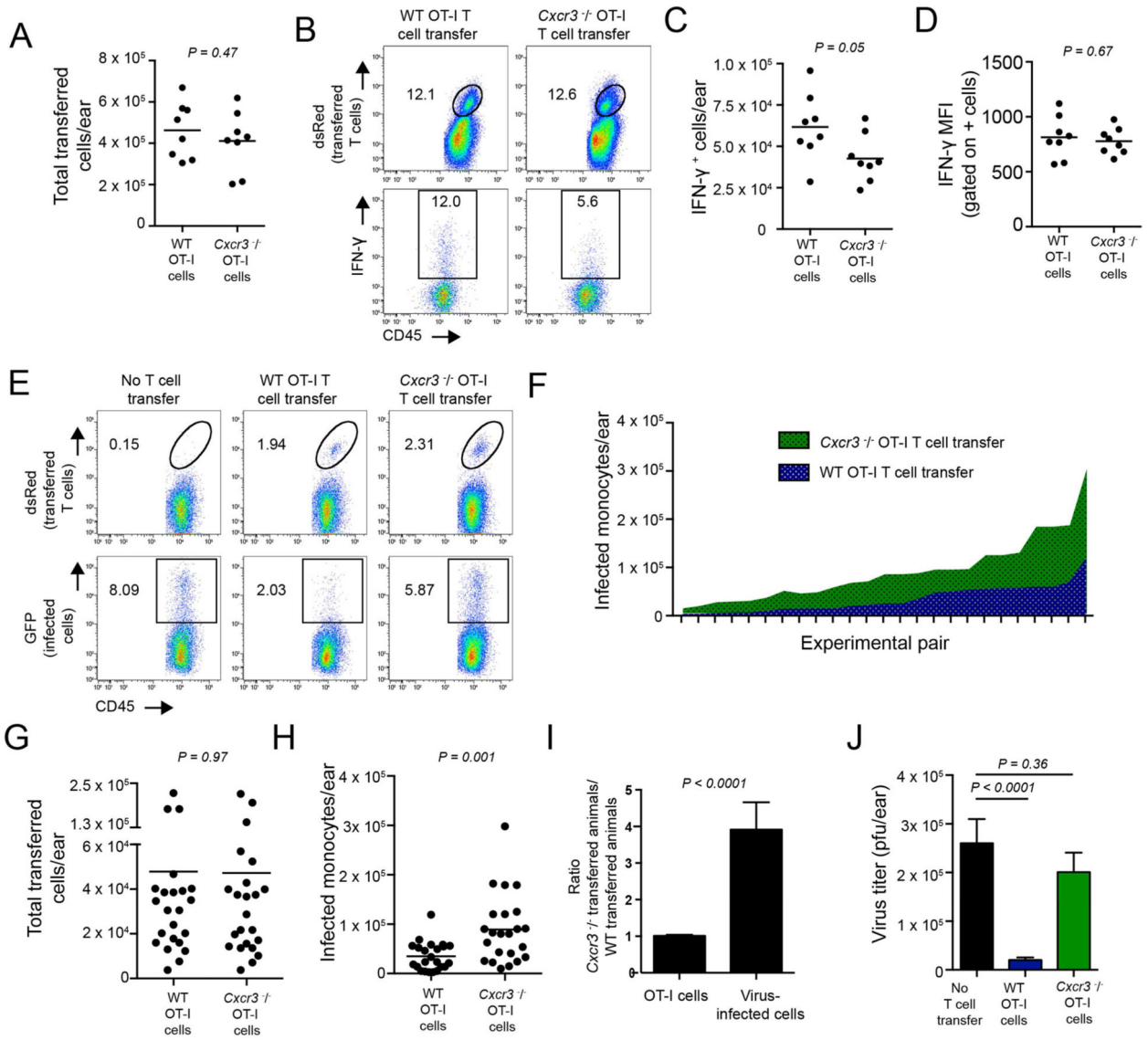

Figure 6. *Cxcr3*$^{-/-}$ CD8^{+} T cells do not kill infected cells as efficiently as WT CD8^{+}T cells

A. Number of WT or *Cxcr3*$^{-/-}$ OT-I CD8^{+} T cells on day 5 p.i. after adoptive transfer into WT animals. Dots = individual ears. **B**. Histograms gated on percentage of transferred T cells (dsRed^{+}, top panels) or on IFN-γ^{+} transferred T cells (bottom panels). WT OT-I cells (left), *Cxcr3*$^{-/-}$ OT-I cells (right). **C.** Number of IFN-γ^{+} cells/ear on day 5 p.i. **D**. Mean fluorescent intensity (MFI) of IFN-γ signal from IFN-γ^{+} population of transferred cells. **E**. Percentage of transferred cells (top panels) recovered in *Cd8*$^{-/-}$ ears after transfer of 2.5 × 10^{5} OT-I cells. No transfer (left panels), WT OT-I cell transfer (middle panels) and *Cxcr3*$^{-/-}$ OT-I transfer (right panels). **F.** Number of infected cells in *Cd8*$^{-/-}$ ears with titrated numbers (from 2.5 × 10^{3} – 7.5 × 10^{5}) of transferred WT (blue) or *Cxcr3*$^{-/-}$ T cells (green). X axis shows pairs of CD8$^{-/-}$ mice in which equivalent numbers of transferred OT-I T cells were recovered. **G**. Number of T cells recovered in *Cd8*$^{-/-}$ mice in experiment shown in F. **H**. Number of infected monocytes per ear from experiment F. **I.** Ratios from mice in F. (Left bar) Number of transferred *Cxcr3*$^{-/-}$ OT-I cells recovered divided by the

number of WT OT-I cells recovered. (Right bar) Number of infected cells under either condition. Statistics in A-C= two-tailed unpaired *t* test. Statistics in F= two-tailed paired *t* test. Error bars = SEM. Experiments A-C were performed 3 times with 3-4 mice/group. Experiments F-G were performed in 5 independent experiments with 2-3 mice/group.

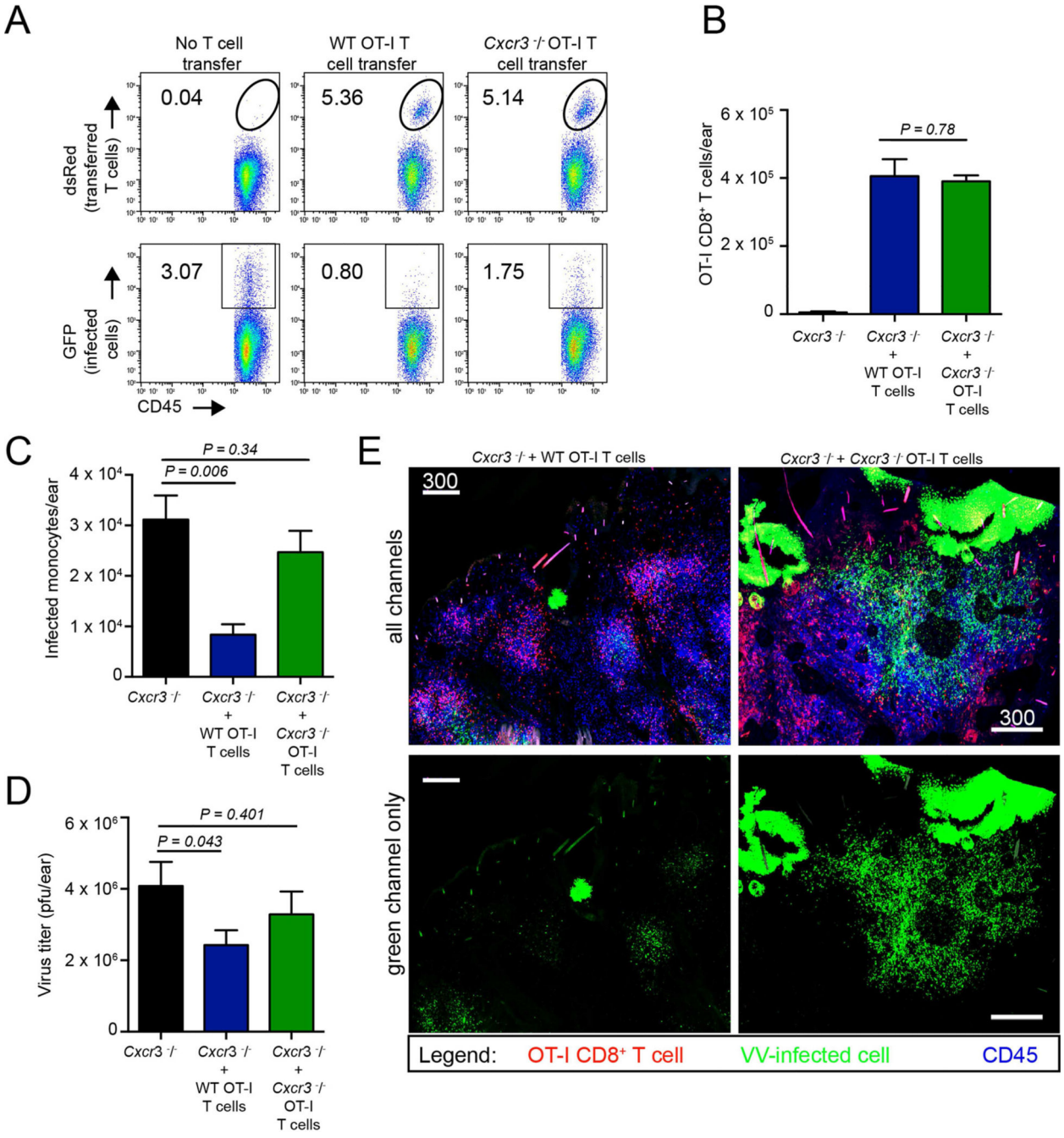

Figure 7. Transfer of WT OT-I CD8$^+$ T cells into *Cxcr3*$^{-/-}$ animals restores viral control

A. Dot plots from *Cxcr3*$^{-/-}$ mice with no T cell transfer (left), or with 2.5 × 10^5 WT (middle) or *Cxcr3*$^{-/-}$ (right) OT-I T cells on 5 days p.i. **B.** Number of adoptively transferred WT or *Cxcr3*$^{-/-}$ OT-I CD8$^+$ T cells recovered per ear in *Cxcr3*$^{-/-}$ animals on day 5 p.i. **C.** Number of virus-infected cells per ear in WT or *Cxcr3*$^{-/-}$ OT-I CD8$^+$ T cell adoptively-transferred *Cxcr3*$^{-/-}$ animals. **D.** Viral titers from C. **E.** Confocal montage images of *Cxcr3*$^{-/-}$ ears 5 days p.i. with VV (green) with transfer of WT or *Cxcr3*$^{-/-}$ OT-I T cells

(red) before infection. $CD45^+$ cells = blue. For clarity, the green channel only is shown in the bottom panels. Statistics= unpaired two-tailed *t* test. Error bars = SEM. Scalebars = μms.